





RESEARCH ARTICLE | OCTOBER 22 2025

Scaling properties of $A + B \rightarrow C$ reaction–diffusion fronts in finite rectilinear geometries **FREE**

D. M. Escala   ; A. De Wit  ; Fabian Brau 



Chaos 35, 103138 (2025)

<https://doi.org/10.1063/5.0291093>



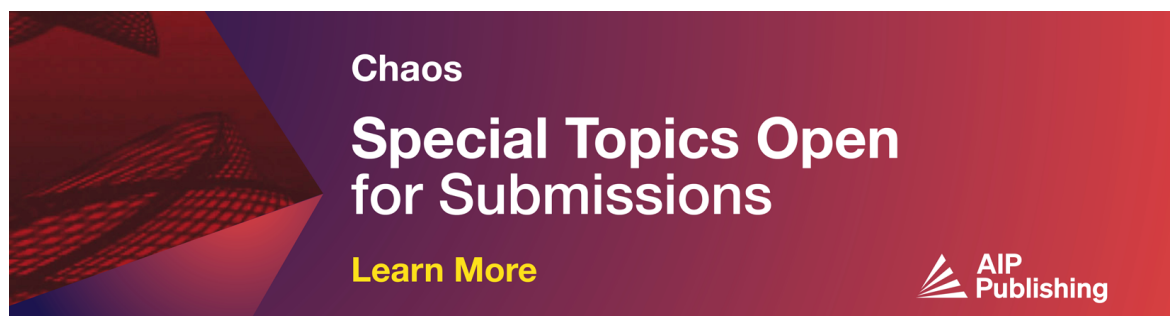
Articles You May Be Interested In

Driven by Brownian motion Cox–Ingersoll–Ross and squared Bessel processes: Interaction and phase transition


Physics of Fluids (January 2025)

The new effect of oscillations of the total angular momentum vector of viscous fluid

Physics of Fluids (August 2022)



Chaos
**Special Topics Open
for Submissions**
[Learn More](#)



Scaling properties of $A + B \rightarrow C$ reaction–diffusion fronts in finite rectilinear geometries

Cite as: Chaos 35, 103138 (2025); doi: 10.1063/5.0291093

Submitted: 15 July 2025 · Accepted: 7 October 2025 ·

Published Online: 22 October 2025



View Online



Export Citation



CrossMark

D. M. Escala,^{a)}  A. De Wit,^{b)}  and Fabian Brau^{c)} 

AFFILIATIONS

Nonlinear Physical Chemistry Unit, Université libre de Bruxelles (ULB), CP231, Boulevard du Triomphe, 1050 Brussels, Belgium

^{a)} Author to whom correspondence should be addressed: dario.martin.escala@ulb.be

^{b)} anne.de.wit@ulb.be

^{c)} fabian.brau@ulb.be

ABSTRACT

$A + B \rightarrow C$ reaction–diffusion fronts are localized reactive zones developing upon diffusive transport and reaction between two zones containing separately the reactants A and B of a bimolecular $A + B \rightarrow C$ reaction. Gálfi and Rácz have characterized the scalings of these types of reaction fronts in infinitely large systems, showing that the position x_f , width w , and maximum production rate R scale as $x_f \sim t^{1/2}$, $w \sim t^{1/6}$, and $R \sim t^{-2/3}$, respectively, where t denotes time. In this work, we show theoretically that the properties of these $A + B \rightarrow C$ reaction–diffusion fronts can be affected in geometries of a finite size. Considering arbitrary finite rectilinear geometry sizes and initial positions of the reactants, we identify the existence of two additional regimes that follow the initial dynamics described by Gálfi and Rácz and are significantly influenced by the geometric constraints of the spatial domain. In the first regime, the observables exhibit an exponential dynamics, while in the second one, the front position remains spatially stationary under certain conditions. We further show that the transition times between regimes depend on the size of the system. We support our calculations with numerical simulations and characterize the dynamics of the front observables as a function of the ratio of initial concentrations.

Published under an exclusive license by AIP Publishing. <https://doi.org/10.1063/5.0291093>

Reaction–diffusion fronts of the type $A + B \rightarrow C$ are fundamental to a wide range of natural and technological processes, from chemistry and biology to ecology and materials science. These fronts typically arise when two initially separated reactants diffuse and react, to create a localized zone of product formation whose properties have been well characterized in infinite systems. However, in practical situations, spatial confinement can profoundly alter the behavior of such reaction fronts. In this work, we theoretically investigate how geometric constraints in finite rectilinear domains affect the scaling properties and temporal evolution of $A + B \rightarrow C$ reaction fronts. We identify and fully characterize two novel temporal regimes that emerge beyond those known for infinite systems, showing how geometric parameters and initial concentrations influence their evolution. Our results are further supported by numerical simulations.

I. INTRODUCTION

Reaction–diffusion (RD) fronts are widely observed across numerous applications, such as pattern formation in geology¹ and

biology,² population dynamics,³ disease spreading,^{4–6} transport of ions in cellular acidity fronts,⁷ nonlinear phenomena in physics,⁸ combustion,⁹ and finance,¹⁰ among others. $A + B \rightarrow C$ fronts represent a significant category of RD fronts that emerge when the reactants A and B, initially segregated in space, diffuse and react to form the product C. Depending on the context and the interpretation of A, B, and C, these fronts can be observed in various systems, including catalysis,¹¹ geochemistry,¹² atmospheric chemistry,¹³ environmental,¹⁴ and ecological¹⁵ problems, among others. One of the foundational works on $A + B \rightarrow C$ RD fronts was conducted by Gálfi and Rácz in 1988.¹⁶ They demonstrated that the temporal evolution of the front position x_f scales as $t^{1/2}$, while the maximum of the production rate $R_f = AB$ and the width w of the front scale as $t^{-2/3}$ and $t^{1/6}$, respectively. These results have been validated numerically,^{17,18} experimentally,¹⁹ and extended to more general cases.^{20–22}

Several studies have investigated the influence of varying parameters, such as initial concentrations and diffusivities of reactants A and B on the front position, showing that certain parameter combinations induce complex dynamics of x_f , causing it to move non-monotonically from its initial position along the

domain.^{23–28} However, most of these studies have assumed either infinite domains or finite geometries with the contact line initially located at the geometric center,^{10,29–31} or they restrict the analysis to short-time regimes where geometric effects are negligible.^{32,33} Recent works have shown that geometry plays a major role in the dynamics of RD fronts in radial^{34,35} and spherical³⁶ advective frameworks. Although these studies demonstrate the universality of the temporal scalings obtained in the pure RD case, the efficiency of the reaction is significantly affected by geometric parameters, which underlines the importance of the geometry in the dynamics of reaction fronts.

In this context, we characterize here the properties of $A + B \rightarrow C$ RD fronts in confined finite rectilinear geometries with arbitrary initial positions of the species and varying geometry sizes. We show the existence of two additional regimes that occur after the dynamics predicted by Gálfi and Rácz, and in which geometric constraints strongly affect the front dynamics. We derive analytical expressions for the temporal scalings in these new regimes and explore the effect of varying the parameters on the front dynamics.

This article is organized as follows: first, we define the finite size geometry parameters and provide a qualitative explanation of the several temporal regimes that will be studied. We review the dynamics in the short and middle times on our finite domain and recall analytical expressions for the characteristic observables. Next, we study the transition and long-time regimes analytically by extending the scaling theory of Gálfi and Rácz in these new temporal regimes. With the obtained analytical expressions, we compute the transition times at which the system switches from one regime to another. In Sec. VII, we study the influence of varying the ratio of initial concentrations on the observables dynamics.

II. NUMERICAL MODEL AND METHODS

We consider a finite, one-dimensional rectilinear domain $x \in [0, L]$, where L is the total system length. In this system, the

chemical species A and B with initial concentrations A_0 and B_0 , respectively, are initially separated at $x = L_0 = L/n$, where n is any number larger than 1 [see Fig. 1(a)]. When $n = 2$ and L is sufficiently large for the dynamics not to be influenced by the borders, we recover the equivalent of the classical infinite system studied by Gálfi and Rácz.¹⁶ Note that the cases $1 < n < 2$ and $n > 2$ are equivalent by symmetry since they can be mapped onto each other by exchanging the roles of species A and B and rescaling the domain. Upon diffusive contact between A and B , the product C is formed through the irreversible bimolecular reaction $A + B \rightarrow C$. The dynamics is governed by the following set of partial differential equations (PDE):

$$\partial_t A = D_A \partial_x^2 A - kAB, \quad \partial_t B = D_B \partial_x^2 B - kAB, \quad \partial_t C = D_C \partial_x^2 C + kAB, \quad (1)$$

where $A = A(x, t)$, $B = B(x, t)$, and $C = C(x, t)$ are the concentration profiles of the chemical species, D_i are their diffusion coefficients, and k is the reaction rate constant. These equations are written in a dimensionless form by rescaling space and time by $\ell = \sqrt{D_A/kA_0}$ and $\tau = 1/kA_0$, respectively. We consider $a = A/A_0$, $b = B/A_0$, and $c = C/A_0$ as the non-dimensional concentration fields and introduce the control parameters $\delta_b = D_B/D_A$, $\delta_c = D_C/D_A$ as the ratios of diffusion coefficients and $\gamma = B_0/A_0$ as the ratio of initial concentrations. We obtain the following dimensionless system of equations:

$$\partial_t a = \partial_x^2 a - ab, \quad \partial_t b = \delta_b \partial_x^2 b - ab, \quad \partial_t c = \delta_c \partial_x^2 c + ab, \quad (2)$$

with no-flux boundary conditions,

$$\begin{aligned} \partial_x a(0, t) &= \partial_x a(L, t) \\ &= \partial_x b(0, t) = \partial_x b(L, t) = \partial_x c(0, t) = \partial_x c(L, t) = 0, \end{aligned} \quad (3)$$

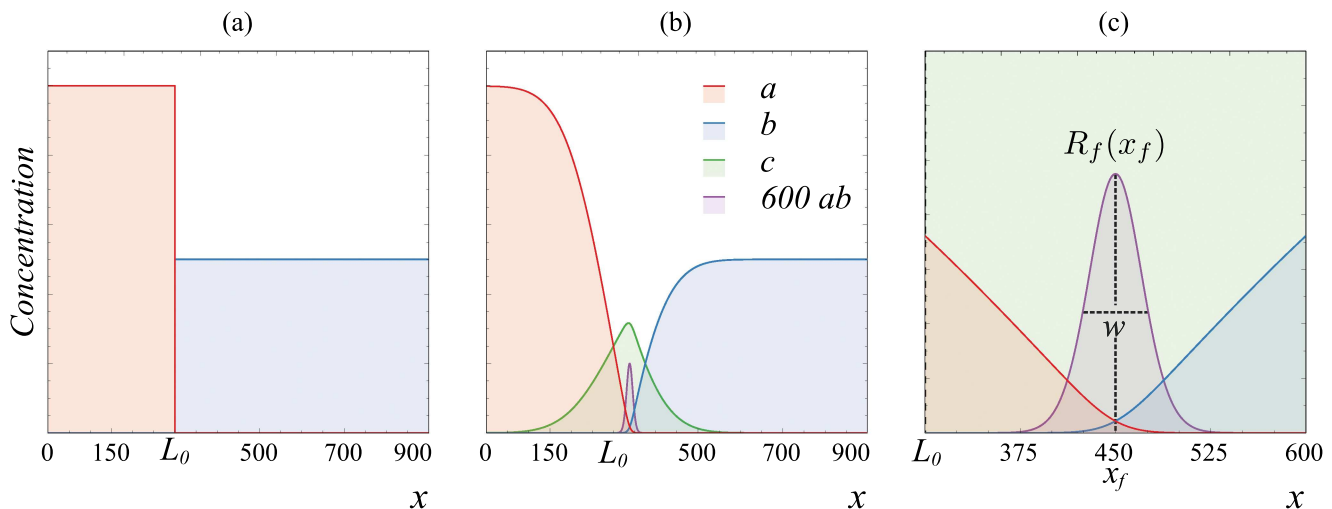


FIG. 1. (a) Spatial concentration profiles a and b at $t=0$. (b) Spatial concentration profiles a , b , and c , and reaction rate $R_f = ab$ at $t=4000$. (c) Closer view near the reaction zone showing the typical observables used to characterize the system: position, maximum, and width of the production rate (x_f , R_f , and w , respectively) in the long-time regime ($t = 2 \times 10^5$). In all figures, $n = 3$, $\delta_b = 1$, $\delta_c = 1$, $\gamma = 0.5$, and $L_0 = 300$.

and initial conditions defined by

$$a(x, 0) = \theta(L_0 - x), \quad b(x, 0) = \gamma\theta(x - L_0), \quad c(x, 0) = 0, \quad (4)$$

where $\theta(x)$ is the Heaviside function.

The equations are solved numerically using the Finite Element Method (FEM) software COMSOL Multiphysics® version 6.0.³⁷ We use the 1-Dimensional Transport of Diluted Species module (tds) with a variable time-stepping method. We discretize the domain using a regular mesh of 20 000 1D elements and set the relative tolerance to 10^{-3} . The final simulation time depends on the values of the parameters, but typically, we use values between 10^5 and 10^7 units of time. To ensure numerical precision and good temporal resolution across all studied regimes, we used a logarithmic time stepping between the initial and final times, with 40 steps per decade. The initial time and the time step were set to 10^{-3} and 10^{-5} , respectively. Note that the product C does not feed back into the reaction front dynamics, and therefore, the effect of varying δ_c is not further discussed in the analysis.

III. TEMPORAL REGIMES AND OBSERVABLES DEFINITION

At the initial time, reactants A and B are put in contact at $x = L_0$ (Fig. 1). Upon reaction and diffusion, a chemical front forms in which the product C is generated. Typical spatial profiles for the concentrations a , b , and c and the reaction rate $R_f = ab$ are shown in Fig. 1(b). Our objective is to analyze the effect that a finite rectilinear geometry produces on the dynamics of the front. To do so, let us study a specific case where $L_0 = 300$, $n = 3$ when $\gamma = 0.5$ (Fig. 1). The system has, thus, a finite size, the initial contact line is not in the middle of the system, and reactants have different initial concentrations. As Fig. 2 shows, we can identify four different temporal regimes. Region I corresponds to the short-time regime, in which diffusion is the driving process. Region II corresponds with the so-called middle-time regime (also known as the

Gálfi and Rácz regime) where diffusion and reaction both control the evolution of the front and finite effects are neglected as the front is still far away from boundaries.^{16,32} In regions I and II, the dynamics of the reaction front is not affected by the geometric constraints and is the same as in an infinitely large domain. For this reason, the temporal scalings in these regions are often studied in the particular case where the species are initially segregated at the geometric center of the domain.^{16,32} As these two regimes were vastly studied in previous works, we will only summarize their properties and adapt the expression of x_f to include the initial position L_0 . Region III corresponds to the transition zone where the dynamics starts to be affected by finite size effects and where the observables switch from a middle- to long-time regime via an exponential dynamics. Finally, in the long-time regime IV, x_f reaches a stationary position depending on the values of parameters, $w(t)$ reaches its maximum value $w^* = L$, and $R(t)$ decreases rapidly to zero (see Fig. 2). This regime IV is more extensive and begins earlier in $x_f(t)$ compared to $w(t)$ or $R(t)$. In Sec. V, we will detail the necessary conditions to obtain an asymptotic stationary front position. It is worth mentioning that once this condition is fulfilled, the dynamics observed in Fig. 2 are similar for any geometry size and initial position.

To characterize the dynamics, we compute observables, such as the position $x_f(t)$, maximum $R(t) = R_f(x_f(t), t) = ab(x_f, t)$, and width $w(t)$ of the production rate $R_f(x, t) = ab$. These observables are shown in Fig. 1(c).¹⁶ To compute $x_f(t)$ from the simulations, we look at the position where $R_f(x, t)$ is maximum. The width $w(t)$ can be computed either as the second moment of the production rate or as the distance at half height of $R_f(x, t)$. Both definitions provide the same trends, but differ by a proportionality constant.

Once we have introduced the characteristic observables and the temporal regimes of interest, we proceed to summarize the findings in regions I and II and present the new results for regions III and IV separately. For simplicity, we assume $\delta_b = 1$ in the forthcoming analysis.

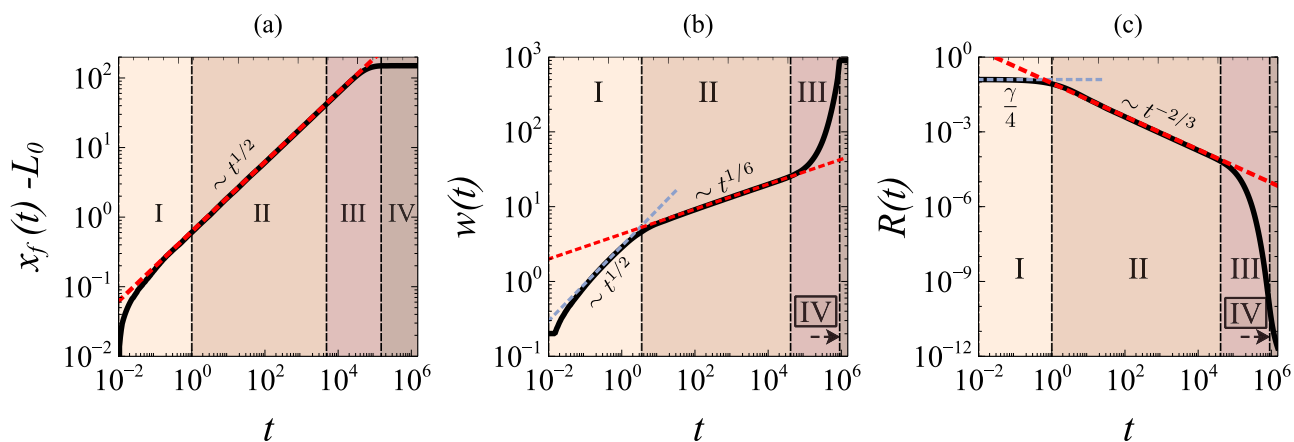


FIG. 2. Dynamics of the reaction front observables corresponding to the profiles shown in Fig. 1 and the four regions described. (a) $x_f(t) - L_0$. We subtract the initial position L_0 to facilitate the observation of the different regimes. (b) Width $w(t)$ and (c) maximum value $R(t)$ of the production rate. The red dashed lines indicate the temporal scalings predicted by Gálfi and Rácz in the middle-time regime.¹⁶ All plots are shown in log scales with $n = 3$, $L_0 = 300$, and $\gamma = 0.5$.

IV. REGIONS I AND II: SHORT- AND MEDIUM-TIME REGIMES

In the early-time regimes, the dynamics are not affected by the boundaries, and thus, the system behaves as if it were infinitely large.^{16,32} In particular, during the short-time regime, diffusion dominates and the reaction terms in Eq. (2) can be neglected. This leads to an uncoupled system of PDEs with well-known analytical diffusive solutions for the concentrations *a* and *b*,

$$a_{st}(x, t) = \frac{1}{2} \operatorname{erfc}(\theta), \quad b_{st}(x, t) = \frac{\gamma}{2} \operatorname{erfc}(-\theta), \quad (5)$$

where the subscript *st* stands for short-time, $\theta = (x - L_0)/(2\sqrt{t})$, and *erfc* denotes the complementary error function.²⁸

Based on Eq. (5), the main observables in the short-time regime can be expressed as

$$x_{fst}(t) = L_0 + \sqrt{2D_f t}, \quad w_{st}(t) = \zeta \sqrt{t}, \quad R_{st}(t) = R^* = \frac{\gamma}{4}, \quad (6)$$

where *D_f* is the solution of the equation $\operatorname{erf}(\sqrt{D_f/2}) = (1 - \gamma)/(1 + \gamma)$. The numerical prefactor ζ in *w_{st}(t)* depends on the definition used: for the width at half maximum, $w_{st}(t) = 4 \operatorname{erf}^{-1}(1/\sqrt{2}) \sqrt{t} \approx 2.97\sqrt{t}$, whereas for the second moment of *ab*, $w_{st}(t) = \sqrt{5/3} \sqrt{t} \approx 1.29\sqrt{t}$.

In the middle-time regime, the analytical expressions for the observables are given by

$$x_{f,mt}(t) = x_{fst}(t), \quad w_{mt}(t) = \frac{\xi}{K_{mt}^{1/3}} t^{1/6}, \quad R_{mt}(t) = \frac{\eta K_{mt}^{A/3}}{t^{2/3}}, \quad (7)$$

where the subscript *mt* refers to middle-time. Here, $K_{mt} = (1 + \gamma)/(2\sqrt{\pi}) e^{-D_f/2}$, while the values of η and ξ are obtained numerically: $\eta \approx 0.298$, while ξ depends on the method used to compute *w(t)*. If the second moment of *R* is used, $\xi \approx 1.37$, whereas if the width at half of the maximum value is used, $\xi \approx 3.11$.^{1,16}

Note that the expression for *x_f(t)* is identical in both short- and middle-time regimes [see the red dashed line in Fig. 2(a)]. Similarly, *w_{st}(t)* and *R_{st}(t)* [Eq. (6)] are shown in Figs. 2(b) and 2(c) as light blue dashed lines, while *w_{mt}(t)* and *R_{mt}(t)* [Eq. (7)] are depicted by red dashed lines.

V. REGIONS III AND IV: TRANSITION AND LONG-TIME REGIMES

We now proceed to study the transition and long-time dynamics beyond the Gálfi and Rác regime, where the finite size of the domain influences the temporal evolution of the observables. We perform the study of these two regimes simultaneously as they both share the same analytical solution, as will be shown below.

A. Analytical solutions

We start our analysis by defining $u_{tr}(x, t) = a(x, t) - b(x, t)$ and assuming equal diffusion coefficients for the species *A* and *B* ($\delta_b = 1$). Subtracting the two first equations in (2) and writing the no-flux boundaries and initial conditions in terms of *u_{tr}*, we obtain

the following PDE system:

$$\begin{aligned} \partial_t u_{tr} &= \partial_x^2 u_{tr}, & \partial_x u_{tr}(0, t) &= \partial_x u_{tr}(L, t) = 0, \\ u_{tr}(x, 0) &= \theta(L_0 - x) - \gamma \theta(x - L_0). \end{aligned} \quad (8)$$

Equation (8) can be solved analytically by the method of separation of variables³⁸ to get

$$\begin{aligned} u_{tr}(x, t) &= \frac{1 + \gamma(1 - n)}{n} \\ &+ \frac{2(\gamma + 1)}{\pi} \sum_{k=1}^{\infty} k^{-1} \sin\left(\frac{\pi k}{n}\right) \cos\left(\frac{\pi k x}{L}\right) e^{-\left(\frac{\pi k}{L}\right)^2 t}, \end{aligned} \quad (9)$$

where the subscript *tr* stands for “transition” and $n = L/L_0$.

B. Temporal scalings

We now proceed to calculate the scalings of the observables in regions III and IV applying the scaling theory of Gálfi and Rác using the analytical expression of *u_{tr}(x, t)* [Eq. (9)].

1. Reaction front position

We note that asymptotically, i.e., for $t \rightarrow \infty$, $u_{tr}(x, \infty) = [1 + \gamma(1 - n)]/n$ is a constant. Therefore, for a given geometry of the domain, i.e., a given $n > 1$, $u_{tr}(x, \infty) > 0$ when $\gamma < \gamma_c$ where

$$\gamma_c = \frac{1}{n - 1}. \quad (10)$$

In this case, all the reactant *B* will be consumed by *A*, and the reaction front position will, thus, move from $x_f = L_0$ at $t = 0$ to $x_f = L$ when $t \rightarrow \infty$. This happens because at $t = 0$, the number of moles of *A* is larger than the number of moles of *B*. Similarly, when $\gamma > \gamma_c$, all the reactant *A* will be consumed by *B*, and the reaction front position will move from $x_f = L_0$ at $t = 0$ to $x_f = 0$ when $t \rightarrow \infty$. On the contrary, when $\gamma = \gamma_c$, the total number of moles of species *A* and *B* are equal at $t = 0$, and the reaction front reaches a stationary position x_f^* in the long-time regime (region IV) after the transition zone (region III). This is easily seen if we say that the numbers of moles of *A* and *B* are equal for a given *L*,

$$a_0 h L_0 = b_0 h (L - L_0) \Rightarrow \gamma \equiv \frac{b_0}{a_0} = \frac{L_0}{L - L_0}, \quad (11)$$

where *h* is the height of a hypothetical rectangular geometry. As we defined the total size of the simulation domain as $L = nL_0$, we obtain that *A* and *B* are initially having the same amount of molecules if $\gamma = \gamma_c$, where

$$\gamma_c = \frac{L_0}{L - L_0} = \frac{L_0}{nL_0 - L_0} = \frac{1}{n - 1}, \quad (12)$$

which is the same expression (Eq. 10) obtained analytically.

To find this stationary position, we need to solve $u_{tr}(x_f^*, t) = 0$ with $\gamma = \gamma_c$. If we keep only the dominant term for $t \gg L^2/(4\pi^2)$ in the sum of Eq. (9), i.e., the term $k = 1$, we find that $u_{tr}(x_f^*, t) = 0$ is equivalent to $\cos(\pi x_f^* L) = 0$ so that $x_f^* = L/2$. To determine how

this asymptotic value of x_f is approached, we need to consider additional terms in the infinite sum of Eq. (9). Actually, it is sufficient to consider the first two terms such that

$$u_{tr}(x, t) \approx \frac{(\gamma_c + 1) e^{-4t(\pi/L)^2}}{\pi} \left(2e^{3t(\pi/L)^2} \sin\left(\frac{\pi}{n}\right) \cos\left(\frac{\pi x}{L}\right) + \sin\left(\frac{2\pi}{n}\right) \cos\left(\frac{2\pi x}{L}\right) \right). \quad (13)$$

The equation $u_{tr}(x_f^*, t) = 0$ can now be written as a second order algebraic equation $2T^2 + AT - 1 = 0$, where $T = \cos(\pi x_f/L)$ and $A = e^{3t(\pi/L)^2} / \cos(\pi/n)$. The two solutions of this equation are given by $T_{\pm} = (-A \pm \sqrt{A^2 + 8})/4$. Assuming $t \gg L^2/(3\pi^2)$, so that A is large, we can expand the expression of T as follows:

$$T_{\pm} \approx \frac{-A \pm |A|(1 + 4/A^2)}{4}. \quad (14)$$

Since we know that $x_f \rightarrow x_f^* = L/2$ when $t \rightarrow \infty$, we also know that $T \rightarrow 0$ when $A \rightarrow \infty$. Therefore, when $A > 0$, ($n > 2$), T_+ is the correct solution, and when $A < 0$, ($1 < n < 2$), T_- is the correct one. In both cases, we obtain $T \equiv \cos(\pi x_f/L) = 1/A$ at the leading order. The solution reads

$$x_{f, tr}(t) = \frac{L}{\pi} \arccos\left(\frac{1}{A}\right) \approx \frac{L}{2} - \frac{L}{\pi A} = \frac{L}{2} - \frac{L}{\pi} \cos\left(\frac{\pi}{n}\right) e^{-3t(\pi/L)^2}, \quad (15)$$

where we have expanded $\arccos(1/A)$ since $A \gg 1$. This represents the expression of $x_f(t)$ for the transition and long-time regimes in a finite system.

Equation (15) shows that, when the initial ratio of concentrations is set to γ_c , the reaction front reaches a stationary position at $x_f^* = L/2$ in the long-time regime, whatever the size of the finite system and the initial position L_0 . In other words, for a finite system of length L , if the initial contact line between A and B is located at $L_0 = L/n$, there exists a critical ratio of initial concentrations $\gamma_c = 1/(n - 1)$ such that the initial number of moles of A equals that of B . Under these conditions, the front evolves toward the stationary position $x_f^* = L/2$ at the center of the domain. This behavior contrasts with infinite systems, where, except for $n = 2$, the front moves indefinitely toward the less concentrated reactant, following the Gálfi and Rácz scalings [Eq. (7)]. This difference can be observed in Fig. 3(a) for various domain sizes. In the long-time regime, the stationary position of the front at $x_f^* = L/2$ can be understood physically: the diffusive fluxes of the reactants ($J_a = -\partial a/\partial x$ and $J_b = -\partial b/\partial x$) at $x = x_f^*$ are equal in magnitude but opposite in direction, ensuring that the supply of both reactants to the reaction zone is balanced and thus maintaining the front at the center of the domain [see Fig. 3(b)]. Finally, Eq. (15) not only predicts the final stationary position x_f^* , but also describes how $x_f(t)$ approaches x_f^* during the transition regime. This dynamical evolution is illustrated in Fig. 3(c), which shows $x_f(t)$ across all time regimes and compares it with the analytical scalings.

2. Maximum and width of the production rate

To compute $R(t)$ and $w(t)$ in the transition and long-time regimes, we follow the same approach as Gálfi and Rácz,¹⁶ adapted to our finite geometry. We summarize the most relevant results, while all the derivations in the scaling analysis are detailed in the [supplementary material](#). We start the analysis expanding $u_{tr}(x, t)$ around the front position $x_f(t)$ and study its behavior in the center of the reaction front,

$$u_{tr}(x, t) \approx (x - x_f(t)) \partial_x u_{tr}(x, t)|_{x=x_f(t)}. \quad (16)$$

Using the leading first term ($k = 1$) in Eq. (9) and considering $\gamma = \gamma_c$, we obtain

$$u_{tr}(x, t) \approx -K_{tr} (x - x_f^*) e^{-(\frac{\pi}{L})^2 t}, \quad K_{tr} = \frac{2}{L} (\gamma_c + 1) \sin\left(\frac{\pi}{n}\right). \quad (17)$$

We introduce the following scaling ansatz for the species A :

$$a(z, t) = g(t)G(z), \quad z = \frac{x - x_f^*}{f(t)}, \quad (18)$$

where it can be shown that

$$f(t) = e^{\frac{1}{3}(\frac{\pi}{L})^2 t}, \quad g(t) = e^{-\frac{2}{3}(\frac{\pi}{L})^2 t}. \quad (19)$$

Applying the boundary conditions for $a(z)$ and assuming that the analysis is done in the transition regime where $w(t) \ll L$ (see the [supplementary material](#) for more details), we obtain a nonlinear differential equation for $G(z)$ identical to that of infinite systems from Gálfi and Rácz,

$$G''(z) = G(z)^2 + K_{tr} z G(z). \quad (20)$$

Solving Eq. (20) numerically and combining with the results from the previous steps, we observe that the maximum production rate and width in the transition regime scale as

$$R_{tr}(t) = \eta K_{tr}^{4/3} e^{-\frac{4}{3}(\frac{\pi}{L})^2 t}, \quad w_{tr}(t) = \xi K_{tr}^{-1/3} e^{\frac{1}{3}(\frac{\pi}{L})^2 t}, \quad (21)$$

where η and ξ are the same values as the medium-time regime expressions [Eq. (7)].¹⁶ Intermediate steps and further mathematical details are provided in the [supplementary material](#).

From Eqs. (15) and (21), we see that in the transition and long-time regimes, the three main observables of the reaction front are a function of the geometric parameters n (through the expression of K_{tr}) and L . Figure 4 compares the numerical computation of $w(t)$ and $R(t)$ with their corresponding analytical expressions for all the described regimes.

VI. TRANSITION TIMES

As we have now obtained analytical expressions for the observables x_f , w , and R in each temporal regime, we can proceed to calculate the transition times between these regimes. We define the transition times as the times when the reaction front switches its dynamics from one regime to another. In this context, it is particularly relevant to analyze how these characteristic times depend on the values of the parameters, especially in the long-time regimes. Therefore, we define $t_{i(st \rightarrow mt)}$ and $t_{i(mt \rightarrow tr)}$ as the times at which

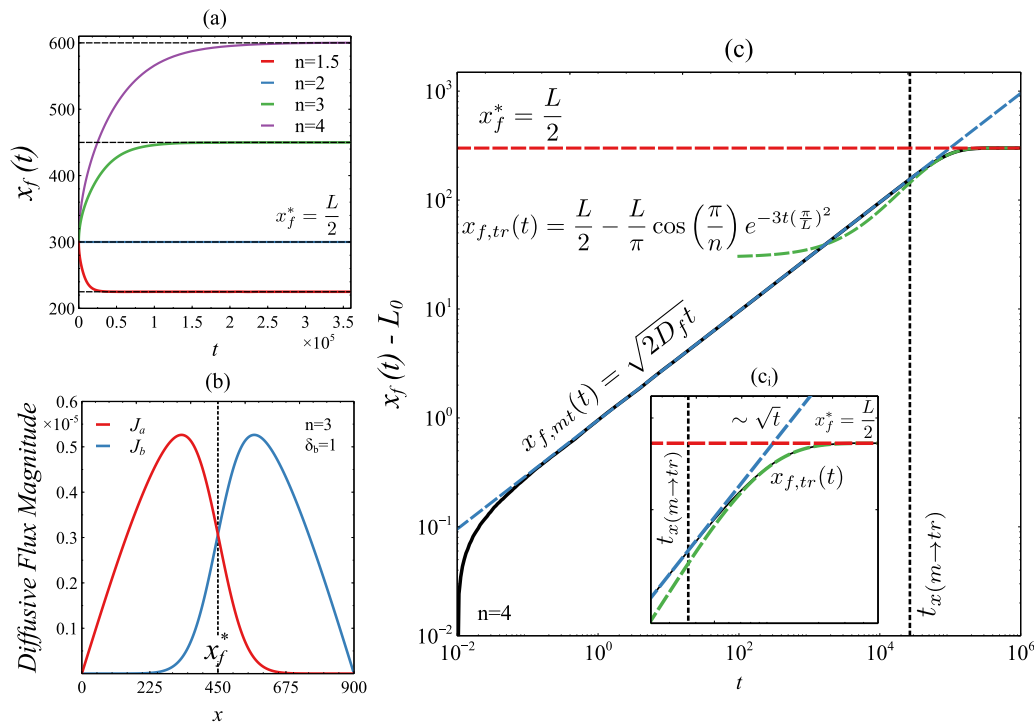


FIG. 3. (a) $x_f(t)$ in the transition and long-time regimes for different finite sizes $L = nL_0$, with $L_0 = 300$ when $\gamma = \gamma_c = 1/(n - 1)$. In this temporal regime, the reaction front remains stationary at $x_f^* = L/2 = nL_0/2$. (b) Plot of the magnitude of the diffusive fluxes of the species A and B as a physical interpretation of x_f^* . In the long-time regime, the front is stationary at the position where $J_a = |J_b|$. The spatial fluxes J_a and J_b were obtained from the numerical simulations. (c) Log-log plot showing all the temporal regimes of $x_f - L_0$ for $n = 4$ (black solid curve). The blue dashed line corresponds to the short- and middle-time regime [Eq. (6)]. The green and red dashed lines correspond to the transition and long-time regimes, respectively [Eq. (15)]. Inset c_i shows a closer view of the transition region. The vertical black dashed lines indicate the times when the system switches from the medium to the transition regime (see Sec. VI for more details).

the observables $i = x, w, R$ transition from the short- to middle-time regime and from the middle- to transition regime, respectively. Additionally, we define t^* as the time at which $w(t) = w^* = L$, i.e., the time at which the front has invaded the whole system. To characterize these transition times, we assume $\gamma = \gamma_c$ and analyze the points at which the analytical expressions for the short-, middle-, and transition-time regimes become equal or as close as possible in time (see Figs. 3 and 4). We first focus on the transition times of $w(t)$ and $R(t)$. Since these observables exhibit well-defined scaling behavior in all temporal regimes, it is possible to determine all relevant transition times analytically. In particular, we obtain $t_{w(st \rightarrow mt)}$ and $t_{R(st \rightarrow mt)}$ by equating w_{st} and R_{st} [Eq. (6)] with their corresponding middle-time regime expressions [Eq. (7)],

$$t_{w(st \rightarrow mt)} = \left[\frac{\xi}{4 \operatorname{erf}^{-1}\left(\frac{1}{\sqrt{2}}\right)} \right]^3 K_{mt}^{-1}, \quad t_{R(st \rightarrow mt)} = K_{mt}^2 \left[\frac{4\eta}{\gamma} \right]^{3/2}. \tag{22}$$

Equation (22) is valid for any γ . Because the reaction front is far from the system boundaries in these regimes, both transition times are independent of the geometric parameters.

For the middle-to-transition regime, the analytical scalings do not intersect. Instead, we estimate the transition time by evaluating when the two expressions are closest. To do so, we define the functions $H_w(t) = w_{tr}(t)/w_{mt}(t)$ and $H_R(t) = R_{mt}(t)/R_{tr}(t)$ and identify the transition times as the moments when these functions reach their minimum values [see Fig. 5(a)]. This approach is necessary because, as shown in Fig. 5(b), $H_w(t)$ and $H_R(t)$ remain greater than one and never cross the value of unity, indicating that the middle- and long-time regime expressions do not intersect in time. By solving for the minima of these functions, we find that both observables share the same transition time,

$$t_{w(mt \rightarrow tr)} = t_{R(mt \rightarrow tr)} = \frac{L^2}{2\pi^2}. \tag{23}$$

Finally, we determine t^* as the time at which $w_{tr}(t) = L$. Solving this condition yields

$$t^* = 3 \frac{L^2}{\pi^2} \ln \left(\frac{K_{tr}^{1/3} L}{\xi} \right). \tag{24}$$

In contrast to Eq. (22), the transition times associated with the long-time regimes depend explicitly on the system size via the factor

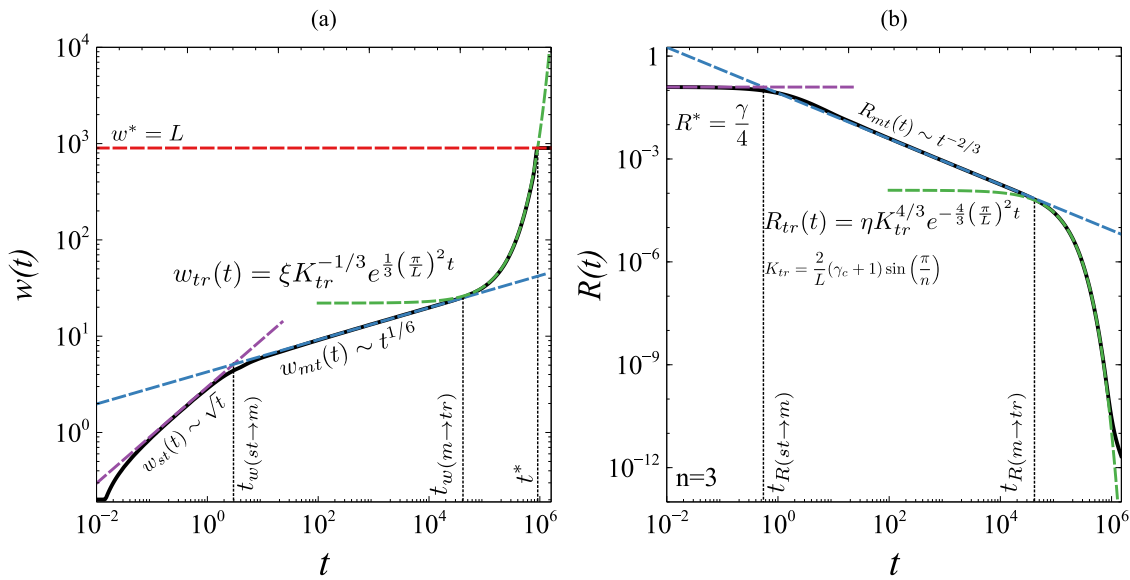


FIG. 4. Temporal evolution of $w(t)$ and $R(t)$ compared with their analytical expressions in all time regimes. (a) $w(t)$ (black solid curve) obtained by measuring the distance at half of the peak. (b) $R(t)$ (black solid curve) calculated numerically as the maximum of ab . Both plots are in log scales to facilitate the observation of short and medium times. In both cases, $L_0 = 300$, $n = 3$, $\gamma = \gamma_c$, $\xi \approx 3.11$, and $\eta \approx 0.298$. The purple, blue, green, and red dashed lines indicate the short, medium, transition, and long-time regimes, respectively. The vertical black dashed lines indicate the times when the system switches between regimes (see Sec. VI for more details).

L^2/π^2 . The transition times of w and R are indicated by black vertical dashed lines in Fig. 4.

We now proceed to study $x_f(t)$. For this observable, there is only one relevant transition time, $t_{x(mt \rightarrow tr)}$, since the short- and medium-time regimes share the same analytical expression [Eqs. (6) and (7)]. Furthermore, it is not possible to define a transition time for the long-time regime in this case, as $x_f^* = L/2$ is only reached asymptotically in the limit $t \rightarrow \infty$ [see Eq. (15)]. To compute $t_{x(mt \rightarrow tr)}$ analytically, we refer to Fig. 3(c), where the different scalings of x_f for $n = 4$ are compared. We first observe that there is a time where $x_{f,mt}(t) = x_{f,tr}(t)$. However, this occurs well before the actual transition region. Moreover, even if this time is taken as a rough approximation for the transition time, the resulting equation is transcendental and, thus, does not yield an analytical solution. For these reasons, we do not consider this intersection as the transition time. Instead, we estimate the transition time for x_f by solving the equation $x_{f,mt}(t) - L_0 = \alpha |x_{f,tr}(t) - L/2|$, where α is a proportionality constant used to adjust the value. For simplicity, we set $\alpha = 1$ [see Fig. 6(a) for a graphical interpretation of the equation]. This equation admits a well-defined analytical solution given by

$$t_{x(mt \rightarrow tr)} = \frac{L^2}{6\pi^2} W_0(M(n)), \quad M(n) = \frac{3}{2} \left(\frac{\cos(\frac{\pi}{n})}{\operatorname{erf}^{-1}(\frac{n-2}{n})} \right)^2, \quad (25)$$

where W_0 denotes the principal branch of the Lambert function, which solves $x = ye^x$. Equation (25) provides a consistent and accurate estimation of the transition time, valid for any $n > 1$ (except for $n = 2$, where $t_{x(mt \rightarrow tr)}$ lacks of any physical meaning), as shown

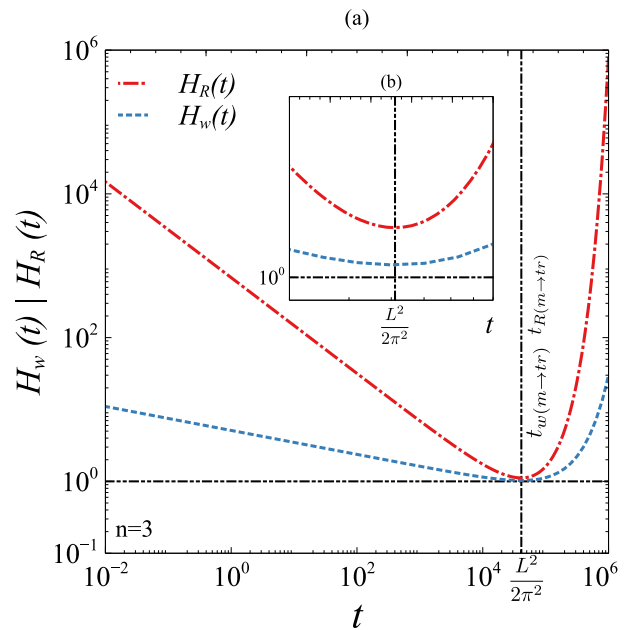


FIG. 5. (a) Graphical interpretation of the transition times $t_{w(st \rightarrow m)}$ and $t_{R(st \rightarrow m)}$ using the functions $H_w(t) = w_{tr}(t)/w_{mt}(t)$ and $H_R(t) = R_{mt}(t)/R_{tr}(t)$, respectively. Both curves attain their minimum at $t = L^2/2\pi^2$. (b) Zoomed view around the transition region, showing that $H_R(t) > H_w(t) > 1$ and confirming that the middle- and long-time analytical expressions never cross in time. In these plots, $n = 3$, $\gamma = \gamma_c$, and $L_0 = 300$.

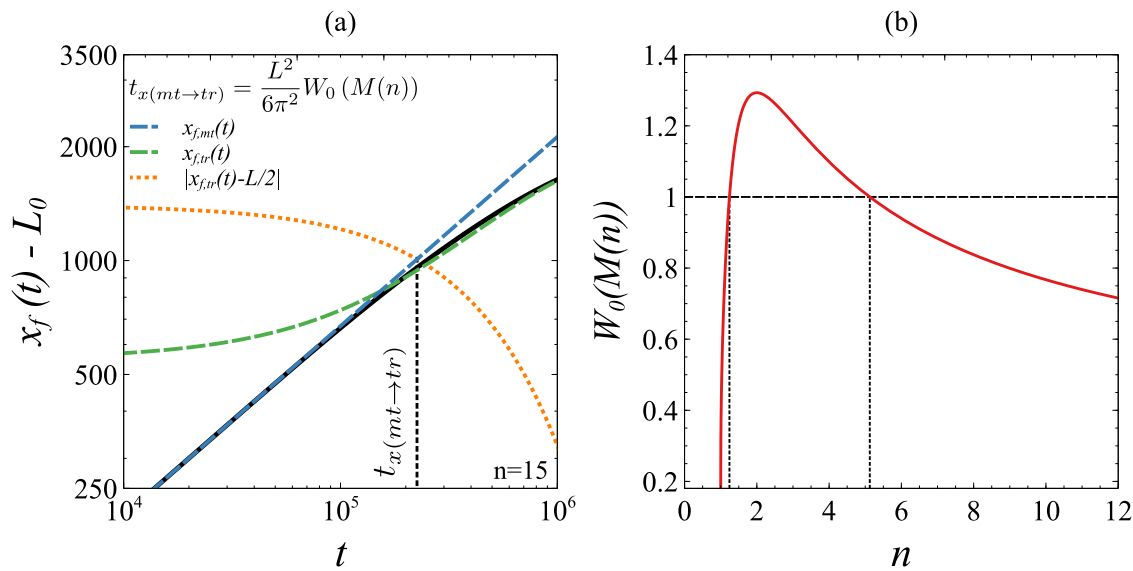


FIG. 6. (a) Graphical interpretation of $t_{x(mt \rightarrow tr)}$ as the solution to $x_{f,ml}(t) - L_0 = |x_{f,tr}(t) - L/2|$. The transition time is indicated by the vertical black dashed line. (b) Plot of $W_0(M(n))$ [Eq. (25)] as a function of n . This expression is valid for any $n > 1$ (with the exception of $n = 2$ in our physical context). The vertical and horizontal lines indicate the values where $t_{x(mt \rightarrow tr)} = L^2/(6\pi^2)$.

in Fig. 6(b). In particular, we note that for $n \approx 1.24$ and $n \approx 5.12$, $t_{x(mt \rightarrow tr)} \rightarrow L^2/(6\pi^2)$.

Despite the differences between the analytical expressions of the temporal scalings, it is noteworthy that all the resulting expressions preserve the characteristic scaling with L^2/π^2 . This recurring spatial dependence suggests a certain universality determined by the finite system size.

VII. EFFECT OF VARYING THE RATIO OF INITIAL CONCENTRATIONS

We now analyze how varying γ affects the dynamics of the reaction front. In this section, we present a general criterion to predict the direction of motion of the reaction front when γ differs from the critical value γ_c , thereby extending previous results obtained for infinite geometries.^{16,17}

Several studies have addressed the influence of γ on the position of the reaction front in the short- and medium-time regimes.^{16,25,26,32} In these works, it has been shown that, in infinitely extended systems, the front remains stationary at the initial contact position ($x = 0$) only if $\gamma = 1$ and $\delta_b = 1$. Otherwise, the front moves to the left or right of $x = 0$ if γ is greater or less than 1, respectively.¹⁸ These results for the short-time regime hold for any γ and any geometry, as boundary effects are negligible. However, we showed that, to observe a stationary front position in the long-time regime, it is necessary to set $\gamma = \gamma_c$. Under this condition, the criterion described for the short-time regime becomes a function of the geometric parameter n : the reaction front moves to the right or left of $x = L_0$ for $n < 2$ or $n > 2$, respectively.

Let us now focus on the long-time regime. For $\gamma = \gamma_c$, $x_f(t)$ will eventually reach a stationary position at $x = L/2$ after the short and

middle times. We can summarize this general dynamics as follows: if the total number of moles of A initially exceeds that of B, the front moves to the right; if B is in excess, it moves to the left; and if both are equal, the front moves toward the center of the domain. If it is already initially centered ($n = 2$), it remains stationary.

We next consider the case $\gamma \approx \gamma_c$, where the front does not reach a stationary position. To investigate this, we use the general solution $u_{tr}(x, t)$ to predict the direction of movement of the reaction front with respect to the stationary position $x_f^* = L/2$. From Eq. (9), retaining only the $k = 1$ term, we obtain

$$u_{tr}(x, t) \approx \frac{1 - \frac{\gamma}{\gamma_c}}{n} + \frac{2}{\pi}(\gamma + 1) \sin\left(\frac{\pi}{n}\right) \cos\left(\frac{\pi x}{L}\right) e^{-\left(\frac{\pi}{L}\right)^2 t}. \quad (26)$$

Solving $u_{tr}(x, t) = 0$ yields $x_{f,tr}(t)$, and differentiating with respect to time leads to

$$x'_{f,tr}(t) = -\beta(t) \left(\frac{\gamma}{\gamma_c} - 1 \right), \quad \beta(t) > 0, \quad (27)$$

which shows that the sign of $x'_{f,tr}(t)$ depends only on the factor $(\gamma/\gamma_c - 1)$. Thus, the analytical expression predicts that the front moves away from its stationary position x_f^* to the left for $\gamma > \gamma_c$, to the right for $\gamma < \gamma_c$, and it remains stationary if $\gamma = \gamma_c$. This analysis demonstrates that any deviation of γ from γ_c will cause the reaction front to move away from its asymptotic stationary position $x_f^* = L/2$, as illustrated in Fig. 7(a). Numerical simulations confirm this prediction. This result generalizes previous findings for infinite systems and provides a general criterion to predict the direction of the front in the long-time regime.^{16,25,26,32}

These results also highlight the interplay between short- and long-time behaviors. For $\gamma \approx \gamma_c$, the initial movement of $x_{f,st}(t)$

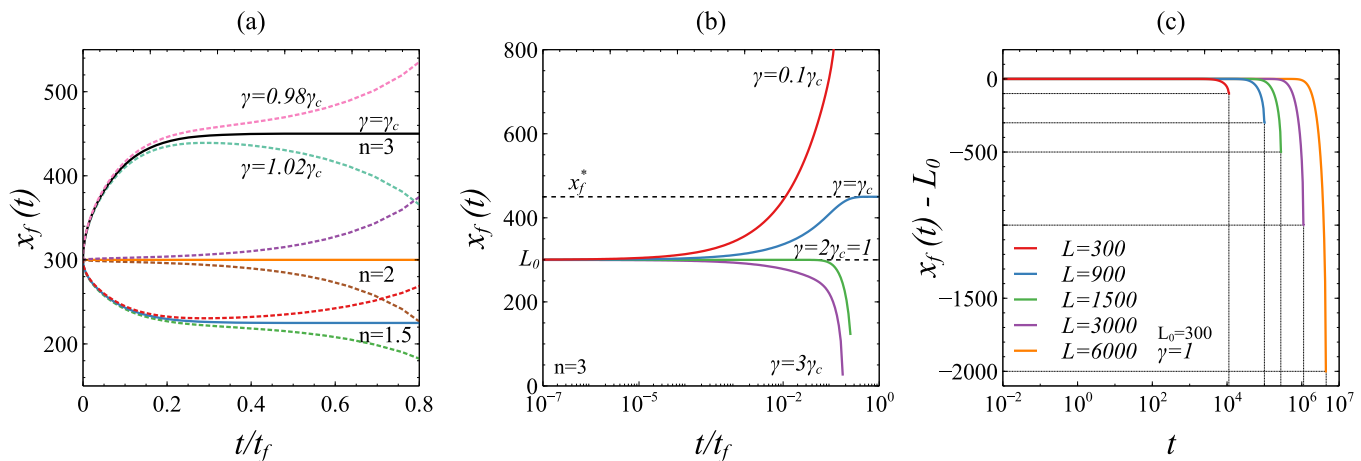


FIG. 7. Dynamics of $x_f(t)$ as a function of γ . (a) For $\gamma \approx \gamma_c$, the short-time dynamics is controlled by the geometric parameter n , while the final position in the long-time regime is set by the value of γ relative to γ_c . (b) When γ deviates from γ_c , the short-time dynamics dominates and the front rapidly moves away from any equilibrium position. For $\gamma = 1$, the front remains temporarily stationary at L_0 until the limiting species is depleted; for $\gamma = \gamma_c$, the front eventually moves to x_f^* in the long-time regime. Plot (b) (for $n = 3$) is shown on log scales to highlight the short-time regime. In both (a) and (b), $L_0 = 300$, and time is normalized by the total simulation time (t_f) for better comparison. (c) Short-time dynamics of $x_f(t)$ as a function of the initial concentration of the limiting species. Horizontal and vertical dashed lines indicate the last tracked position of x_f and the corresponding time, respectively. The time for which the front remains at its initial position increases with the total concentration of the limiting species, which in this case is proportional to L_0 . All cases correspond to $n = 3$ and $\gamma = 1$. Curves have been shifted to the initial position for a better comparison.

depends only on the initial position L_0 (which fixes $n = L_0/L$) as seen at earlier times in Fig. 7(a). Thus, if $n = 2$, $\gamma_c = 1$ and the front does not move while as soon as $n \neq 1$, $\gamma_c \neq 1$, the front moves toward the less concentrated reactant. In contrast, the asymptotic position in the long-time regime is governed by Eq. (27) and depends on the exact value of γ . Therefore, the direction of motion in the long-time regime is independent of the initial direction in the short-time regime. By varying γ , it is possible to induce non-monotonic front dynamics even if diffusion coefficients are equal, as illustrated in Fig. 7.

Let us now consider the case where γ differs significantly from γ_c . In this scenario, the short-time regime dominates and the behavior of $x_f(t)$ is determined primarily by the value of γ . Specifically, the front moves to the left, right, or remains at L_0 (for a limited time), depending on whether γ is greater than, less than, or equal to 1, respectively [see Fig. 7(b)]. For $\gamma = 1$, one might expect the dynamics observed in infinite domains to be recovered as the system size increases.^{16,18} However, except for $n = 2$ (where species are distributed symmetrically), there is always a limiting reactant on one side of $x = L_0$. As the reaction consumes this limiting species, a flux imbalance develops and pushes the front away from L_0 toward the boundary. Increasing the total concentration of the limiting species increases the time during which the front remains at its initial position. In the limit $|x| \rightarrow \infty$, there is no limiting species, and $x_f(t)$ remains fixed at L_0 . Figure 7(c) compares $x_f(t)$ for different total lengths L of the domain when $n = 3$ and $\gamma = 1$. As shown, the time during which the front remains at L_0 is proportional to L and the fact that the front does not move as $\gamma = 1$ is recovered in the limit $L \rightarrow \infty$ (the Gálfi and Rácz case)

Finally, we can analytically demonstrate that the only situation in which the front remains indefinitely at its initial position is when

$x_f^* = L_0$, which requires $nL_0/2 = L_0$, or, equivalently, $n = 2$. For any other value of n , even if $\gamma = 1$, the front will eventually leave L_0 once the limiting species is consumed (see Fig. 7).

VIII. DISCUSSION

We now discuss the feasibility of observing the transition and long-time regimes in real systems. As an example, consider a fast $A + B \rightarrow C$ reaction with a kinetic constant of $k = 200 \text{ M}^{-1} \text{ s}^{-1}$ and diffusion coefficients $D_A = D_B = D_C = 3 \times 10^{-9} \text{ m}^2/\text{s}$. These values are chosen as generic parameters of a representative well studied bimolecular reaction front.³⁹ For a small capillary of length $L = 3 \text{ cm}$, with $L_0 = 1 \text{ cm}$ and initial concentrations $A_0 = 1 \text{ M}$ and $B_0 = 0.5 \text{ M}$ ($n = 3$), the reaction front would enter the transition regime after approximately 3 h and reach the stationary position x_f^* after about 15 h. It is important to note that the dimensional transition times scale with L^2/D , indicating that these times depend exclusively on the diffusivity of the reactants, while the reaction kinetics become irrelevant in the long-time regime. Consequently, the transition and long-time regimes could be observed more rapidly in experiments where the reactants diffuse faster, either due to the nature of the molecules or the properties of the medium.

Note that the applicability of our findings is not limited to chemical reactions in liquid or gel media. Similar reaction-diffusion dynamics of the $A + B \rightarrow C$ type are relevant in a variety of other fields, such as ecology (e.g., the spatial spread of populations or diseases), materials science (e.g., pattern formation during synthesis in porous solids or gels), and developmental biology (e.g., morphogen gradients in tissues). In these contexts, the relevant timescales can be different, or the transport processes may be controlled to make the different dynamical regimes accessible. Thus,

the theoretical framework and analytical results presented here may provide insights that extend far beyond purely chemical applications. In particular, these considerations highlight the direct applicability of our finite-geometry scaling laws to realistic experimental systems and interdisciplinary contexts where confinement plays a key role.

More extensively, the existence of transition and long-time regimes could play a key role in any process modeled by $A + B \rightarrow C$ kinetics, particularly in finite domains or under time-dependent conditions. Our results contribute to understand reaction–diffusion fronts not only in rectilinear but also in other types of finite geometries, and under external constraints that could impact front propagation.

IX. CONCLUSIONS

We have theoretically investigated the effect of finite geometries on the dynamics of $A + B \rightarrow C$ reaction fronts. We have shown that, depending on the initial values of the parameters, the front dynamics can differ from those described for infinite systems or from the special case where the reactants are initially positioned at the geometric center of the domain ($n = 2$).

We identified the existence of a critical initial concentration ratio, γ_c , that controls the dynamics of the reaction front at long times. When $\gamma = \gamma_c$ and $n > 1$, the reaction front exhibits two additional temporal regimes, the transition and long-time regimes, that extend the dynamics described by Gálfi and Rácz. By extending scaling theory, we derived analytical expressions for these regimes and demonstrated their dependence on the values of the geometric parameters. In the transition regime, observables vary exponentially with time, while in the long-time regime, the location of maximal production rate $R_f(x, t) = ab$ converges to the stationary position $x_f^* = L/2$.

By comparing short- and long-time regimes, we have characterized the influence of varying γ on front dynamics, generalizing the classical analysis for infinite domains and providing new criteria to predict the direction of front propagation based on the initial concentration ratio. The critical role of γ_c in the non-monotonic long-time behavior of x_f^* has also been highlighted.

It is important to note that the present model relies on certain simplifying assumptions, such as irreversible reaction, equal diffusion coefficients for all species, and the absence of convective⁴⁰ or external effects. In real systems, deviations from these assumptions may lead to qualitatively different dynamics, especially over long timescales or in more complex environments. Future work could address these factors by considering reversible reactions, unequal diffusivities, or the influence of external fields, boundary fluxes, or fixed concentrations in rectilinear, radial, or even spherical finite geometries.

Overall, this study provides a theoretical framework for understanding and predicting the behavior of $A + B \rightarrow C$ reaction fronts in finite systems, opening the door to a wide range of future investigations and applications in both fundamental and applied contexts.

SUPPLEMENTARY MATERIAL

See the [supplementary material](#) for a detailed version of the scaling analysis presented in Sec. [V B 2](#).

DEDICATION

This work is dedicated to the loving memory of Professor Pedro Luis Pascual.

ACKNOWLEDGMENTS

The authors acknowledge the financial support of Prodex (Belgium) under Grant No. 4000144733.

AUTHOR DECLARATIONS

Conflict of Interest

The authors have no conflicts to disclose.

Author Contributions

D. M. Escala: Investigation (lead); Writing – original draft (lead). **A. De Wit:** Conceptualization (supporting); Supervision (supporting); Writing – review & editing (supporting). **Fabian Brau:** Supervision (supporting); Writing – review & editing (supporting).

DATA AVAILABILITY

The data that support the findings of this study are available from the corresponding author upon reasonable request.

REFERENCES

- ¹T. Antal, M. Droz, J. Magnin, and Z. Rácz, “Formation of Liesegang patterns: A spinodal decomposition scenario,” *Phys. Rev. Lett.* **83**, 2880 (1999).
- ²S. Kondo and T. Miura, “Reaction-diffusion model as a framework for understanding biological pattern formation,” *Science* **329**, 1616–1620 (2010).
- ³J. D. Murray, *Mathematical Biology* (Springer, Berlin, 2003).
- ⁴J. V. Noble, “Geographic and temporal development of plagues,” *Nature* **250**, 726–729 (1974).
- ⁵V. Belik, T. Geisel, and D. Brockmann, “Natural human mobility patterns and spatial spread of infectious diseases,” *Phys. Rev. X* **1**, 011001 (2011).
- ⁶R. M. Anderson and R. M. May, *Infectious Diseases of Humans: Dynamics and Control* (Oxford University Press, 1991).
- ⁷A. Tóth, I. Lagzi, and D. Horváth, “Pattern formation in reaction-diffusion systems: Cellular acidity fronts,” *J. Phys. Chem.* **100**, 14837–14839 (1996).
- ⁸U. Ebert and W. van Saarloos, “Front propagation into unstable states: Universal algebraic convergence towards uniformly translating pulled fronts,” *Physica D* **146**, 1–99 (2000).
- ⁹F. A. Williams, *Combustion Theory* (CRC Press, 2018).
- ¹⁰I. Mastromatteo, B. Tóth, and J.-P. Bouchaud, “Anomalous impact in reaction-diffusion financial models,” *Phys. Rev. Lett.* **113**, 268701 (2014).
- ¹¹B. Heidel, C. M. Knobler, R. Hilfer, and R. Bruinsma, “Pattern formation at liquid interfaces,” *Phys. Rev. Lett.* **60**, 2492–2495 (1988).
- ¹²P. J. Ortoleva, *Geochemical Self-Organization* (Oxford University Press, Oxford, 1994).
- ¹³J. H. Seinfeld and S. N. Pandis, *Atmospheric Chemistry and Physics: From Air Pollution to Climate Change* (John Wiley & Sons, New York, 2016).
- ¹⁴E. R. Abraham, “The generation of plankton patchiness by turbulent stirring,” *Nature* **391**, 577–580 (1998).
- ¹⁵A. Okubo and S. A. Levin, *Diffusion and Ecological Problems: Modern Perspectives* (Springer Science and Business Media, 2013), Vol. 14.
- ¹⁶L. Gálfi and Z. Rácz, “Properties of the reaction front in an $A + B \rightarrow C$ type reaction-diffusion process,” *Phys. Rev. A* **38**, 3151 (1988).
- ¹⁷H. Taitelbaum, A. Yen, R. Kopelman, S. Havlin, and G. H. Weiss, “Effects of bias on the kinetics of $A + B \rightarrow C$ with initially separated reactants,” *Phys. Rev. E* **54**, 5942 (1996).

- ¹⁸Z. Jiang and C. Ebner, "Simulation study of reaction fronts," *Phys. Rev. A* **42**, 7483 (1990).
- ¹⁹Y. Koo, L. Li, and R. Kopelman, "Reaction front dynamics in diffusion-controlled particle-antiparticle annihilation: Experiments and simulations," *Mol. Cryst. Liq. Cryst.* **183**, 187–192 (1990).
- ²⁰S. Cornell and M. Droz, "Steady-state reaction-diffusion front scaling for $mA + nB \rightarrow [\text{inert}]$," *Phys. Rev. Lett.* **70**, 3824 (1993).
- ²¹S. Cornell, Z. Koza, and M. Droz, "Dynamic multiscaling of the reaction-diffusion front for $mA + nB \rightarrow 0$," *Phys. Rev. E* **52**, 3500 (1995).
- ²²P. Krapivsky, "Diffusion-limited annihilation with initially separated reactants," *Phys. Rev. E* **51**, 4774 (1995).
- ²³E. Ben-Naim and S. Redner, "Inhomogeneous two-species annihilation in the steady state," *J. Phys. A: Math. Gen.* **25**, L575 (1992).
- ²⁴H. Larralde, M. Araujo, S. Havlin, and H. E. Stanley, "Reaction front for $A + B \rightarrow C$ diffusion-reaction systems with initially separated reactants," *Phys. Rev. A* **46**, 855 (1992).
- ²⁵H. Taitelbaum, Y.-E. L. Koo, S. Havlin, R. Kopelman, and G. H. Weiss, "Exotic behavior of the reaction front in the $A + B \rightarrow C$ reaction-diffusion system," *Phys. Rev. A* **46**, 2151 (1992).
- ²⁶Z. Koza and H. Taitelbaum, "Motion of the reaction front in the $A + B \rightarrow C$ reaction-diffusion system," *Phys. Rev. E* **54**, R1040 (1996).
- ²⁷Z. Koza, "The long-time behavior of initially separated $A + B \rightarrow 0$ reaction-diffusion systems with arbitrary diffusion constants," *J. Stat. Phys.* **85**, 179–191 (1996).
- ²⁸V. Mal'yutin, S. Rabinovich, and S. Havlin, "Reaction diffusion with initially separated reactants: Functional integral approach," *Phys. Rev. E* **56**, 708 (1997).
- ²⁹B. M. Shipilevsky, "Death of an a -particle island in the b -particle sea: Propagation and evolution of the reaction front $a + b \leftrightarrow c$," *Phys. Rev. E* **79**, 021117 (2009).
- ³⁰R. Tiani and L. Rongy, "Complex dynamics of interacting fronts in a simple $A + B \rightarrow C$ reaction-diffusion system," *Phys. Rev. E* **100**, 030201 (2019).
- ³¹S. Generalis, A. De Wit, and P. Trevelyan, "Exotic dynamics of bimolecular reaction-diffusion fronts in immiscible systems," *Appl. Math. Lett.* **146**, 108821 (2023).
- ³²H. Taitelbaum, "Segregation in reaction-diffusion systems," *Physica A* **200**, 155–164 (1993).
- ³³P. M. J. Trevelyan, "Analytical small-time asymptotic properties of $A + B \rightarrow C$ fronts," *Phys. Rev. E* **80**, 046118 (2009).
- ³⁴F. Brau, G. Schuszter, and A. De Wit, "Flow control of $A + B \rightarrow C$ fronts by radial injection," *Phys. Rev. Lett.* **118**, 134101 (2017).
- ³⁵F. Brau and A. De Wit, "Influence of rectilinear vs radial advection on the yield of $A + B \rightarrow C$ reaction fronts: A comparison," *J. Chem. Phys.* **152**, 054716 (2020).
- ³⁶A. Comolli, A. De Wit, and F. Brau, "Dynamics of $A + B \rightarrow C$ reaction fronts under radial advection in three dimensions," *Phys. Rev. E* **100**, 052213 (2019).
- ³⁷COMSOL Multiphysics® version 6.0, COMSOL AB, Stockholm, Sweden.
- ³⁸L. Debnath, *Nonlinear Partial Differential Equations for Scientists and Engineers* (Birkhäuser, Boston, MA, 2012).
- ³⁹A. Tóth, G. Schuszter, N. P. Das, E. Lantos, D. Horváth, A. De Wit, and F. Brau, "Effects of radial injection and solution thickness on the dynamics of confined $A + B \rightarrow C$ chemical fronts," *Phys. Chem. Chem. Phys.* **22**, 10278–10285 (2020).
- ⁴⁰L. Rongy, P. Trevelyan, and A. De Wit, "Dynamics of $A + B \rightarrow C$ reaction fronts in the presence of buoyancy-driven convection," *Phys. Rev. Lett.* **101**, 084503 (2008).